PandaX-4T limits on Z' mass in 3-3-1LHN model

Vinícius Oliveira[*] and C. A. de S. Pires[†]

Departamento de Física, Universidade Federal da Paraíba, Caixa Postal 5008, 58051-970 João Pessoa - PB, Brazil

(Received 18 January 2022; accepted 15 July 2022; published 29 July 2022)

The framework of the so-called 3-3-1LHN model accommodates two different, but viable, scenarios of dark matter. In one case, the dark matter particle is a heavy Dirac neutrino N_1. In the other case, we have a scalar, ϕ, as a dark matter candidate. In both cases, the dark matter phenomenology, relic abundance, and scattering cross section off of nuclei are controlled by exchange of Z'. We then investigate the impact on the parameter space $(M_{Z'}, M_{(N_1,\phi)})$ due to the recent PandaX-4T experimental result in both scenarios. We obtain that the PandaX-4T experiment excludes scenarios with dark matter mass below 1.9 TeV. Concerning Z', we find the lower bound $M_{Z'} > 4.1$ TeV for the case where N_1 is the dark matter and $M_{Z'} > 5.7$ TeV for the other case. This implies that the 3-3-1 symmetry is spontaneously broken above 10 TeV scale. We also comment on the contributions to the relic abundance of processes involving flavor-changing neutral current mediated by Z'.

DOI: 10.1103/PhysRevD.106.015031

I. INTRODUCTION

The nature of dark matter (DM) continues to be a challenge to particle physics. At the moment, experiments keep making great effort in trying to decipher its nature by means of many types of detection [1–3] (direct, indirect, and collider), while theorists interpret their results inside theories that pose DM particles. Recently, the PandaX-4T [4] experiment released its first report concerning dark matter search by means of direct detection. Its null result translates in a stringent limit to the dark matter–nucleon spin-independent interactions.

The 3-3-1 with left-handed neutrino (3-3-1LHN) model is an interesting dark matter model [5–17]. It is based on the $SU(3)_C \times SU(3)_L \times U(1)_N$ (3-3-1) gauge symmetry [18,19], which poses heavy Dirac neutrinos in its particle spectrum. It carries three DM candidates in its particle spectrum, namely, U^0, N_1, and ϕ. The first is extremely underabundant, while the other two, N_1 and ϕ, are viable DM candidates. Of course they cannot coexist. A kind of R parity guarantees the stability of such DM particles. In this work, we calculate, for both dark matter cases, the relic abundance including flavor-changing neutral process with Z' and extract bounds on the mass of Z' by confronting the theoretical scattering cross section off of nuclei with the PandaX-4T result.

We organize this work in the following way. In Sec. II, we present the essence of the model. In Sec. III, we investigate the dark matter relic abundance and direct detection experiment. Lastly, we summarize and draw our conclusions in Sec. IV.

II. ESSENCE OF THE 3-3-1LHN MODEL

In the 3-3-1LHN model, the left-handed leptons come in triplet representation, $f_{a_L} = (\nu_a, e_a, N_a)^T_L$ $(a = 1, 2, 3)$. For the quark sector, the third generation comes in the triplet representation $Q_{3_L} = (u_3, d_3, u'_3)^T_L$, while the other two come in an antitriplet representation of $SU(3)_L$, $Q_{i_L} = (d_i, -u_i, d'_i)_L$ $(\mathrm{i} = 1, 2)$, as required by anomaly cancellation. With exception of ν_L, all the left-handed fermions have their right-handed counterpart [19]. The new leptons and quarks are heavy particles with their masses belonging to the 3-3-1 energy scale. For all these features and the transformations of these fields by the 3-3-1 symmetry, see Refs. [18,19].

The gauge sector of the model is composed of nine gauge bosons and involves the standard ones $W^{\pm}$, Z, and γ and five others called $W'^{\pm}$, U^0, $U^{0\dagger}$, and Z'. For their masses and features, see Refs. [19,20]. The interactions of these gauge bosons with all the fermions of the model are found in Table I and Eq. (7) of the paper [8]. We use those interactions here.

With the triplet of scalars $\eta = (\eta^0, \eta^-, \eta'^0)^T$, $\rho = (\rho^+, \rho^0, \rho'^+)^T$, and $(\chi^0, \chi^-, \chi'^0)^T$ the symmetries of the model are correctly broken, and mass is generated for

[*]vlbo@academico.ufpb.br
[†]cpires@fisica.ufpb.br

all particles. The potential composed of these triplets of scalars was developed in Ref. [21].

We remark that the 3-3-1LHN model has three viable DM candidates, namely, U^0, N, and ϕ. Their stability is guaranteed by a kind of discrete R-odd parity symmetry $P = (-1)^{3(B-L)+2s}$, where B is the baryon number, L is the lepton number, and s is the spin of the corresponding field. By means of this symmetry, the model poses a set of 3-3-1 particles that transform as follows:

$$(N_L, N_R, d_i', u_3' \rho'^+, \eta'^0, \chi^0, \chi^-, W'^+, U^{0\dagger}) \to -1. \quad (1)$$

We refer to these particles as R-odd particles. All the other particles of the model transform trivially under R-odd parity. Then, the electrically neutral R-odd particles N_1, η'^0, and U^0 are potential dark matter candidates.[1] The gauge boson U^0 is extremely underabundant and naturally discarded as dark matter. Regarding to N_1 and η'^0, they interact one with another by means of the term $\frac{g_{11}' v}{2 v_{\chi'}} \bar{\nu}_e N_1 \eta'^0$ [7]. By enforcing that one of them is the lightest R-odd particle, then, it gets stable and becomes a good dark matter candidate. In what follows, we obtain the abundance of each candidate, their spin independent cross section and confront them with the recent PandaX-4T.[2]

III. RELIC ABUNDANCE AND DIRECT DETECTION

The marvelous characteristic of Weakly interacting massive particles (WIMPs) is that their interactions manifest at the electroweak scale, which naturally leads to the appropriate relic density. Because of this characteristic, the WIMP tends to thermalize with the standard model particles in the primordial Universe. This happens when its interaction rate is greater than the expansion rate of the Universe. The WIMP decouples from the thermal bath when the rate of interactions drops below the expansion rate of the Universe, being cosmologically stable, its abundance keeps constant in the Universe up to today. Additionally, the electroweak scale of WIMPs interaction implies that it is experimentally accessible. Nowadays, there are three potential ways to search these particles experimentally [1,2,22,23], that is, indirectly, directly, or collider. In this work, we will explore the bounds of the direct detection experiment PandaX-4T [4] and, more remarkably, constrain the mass of Z'.

A. Relic abundance

To obtain the WIMP abundance, we need to solve the Boltzmann equation which gives the evolution of the abundance of a generic species in the Universe as a function of the temperature,

$$\frac{dY}{dT} = \sqrt{\frac{\pi g_*(T)}{45}} M_p - \langle \sigma v \rangle (Y^2 - Y_{\rm eq}^2), \quad (2)$$

where g_* is the effective number of degrees of freedom, M_p is the Planck mass, $Y \equiv n/s$ is the abundance or number density (n) over entropy density (s) (while $Y_{\rm eq}$ is the abundance at the equilibrium), and $\langle \sigma v \rangle$ is the thermally averaged cross section for WIMP annihilation times the relative velocity.

The particle physics information of the model enters in the thermally averaged cross section which includes all annihilation and coannihilation channels. In this work, we will assume that $M_{N_1} \ll M_{N_2} \ll M_{N_3}$, which makes the coannihilation processes irrelevant[3] [24]. The thermally averaged cross section for annihilation processes ($A + A \to B + B$) is

$$\langle \sigma v \rangle \equiv \frac{1}{(n_A^{\rm eq}(T))^2} \frac{\mathcal{S}}{32(2\pi)^6} T \int ds \frac{\sqrt{\lambda(s, m_A^2, m_A^2)}}{s} \times \frac{\sqrt{\lambda(s, m_B^2, m_B^2)}}{\sqrt{s}} K_1\left(\frac{\sqrt{s}}{T}\right) \int d\Omega |\mathcal{M}|^2, \quad (3)$$

where $\mathcal{S}$ is the symmetrization factor, T is the thermal bath temperature, s is the Mandelstam variable, $\lambda(x, y, z)$ is the Källén function, K_1 is the modified Bessel function of the second kind of order 1, Ω is the solid angle between initial and final states in the center-of-mass frame, and $|\mathcal{M}|^2$ is the (not averaged) squared amplitude of the process.

The final relic abundance of a DM candidate is defined to be

$$\frac{\Omega^0 h^2}{0.11} \simeq \frac{M_{\rm DM}}{1\ {\rm GeV}} \frac{Y^0}{4.34 \times 10^{-10}}, \quad (4)$$

where $M_{\rm DM}$ represents the DM mass and the label ^{0} indicates quantities as measured today, with $\Omega_{\rm DM}^0 h^2 \simeq 0.11$ being inferred by the Planck satellite [25]. The Y^0 can be obtained by integrating Eq. (2) from $T = T_0$ to $T = \infty$, where T_0 is the temperature of the Universe today.

Our results are obtained by using the package micrOMEGAs [26], which computes the relic density numerically for a given model. The relevant processes which contribute to the abundance of our DM candidates, N_1 and ϕ, separately, are shown in Figs. 1 and 2. However, other interactions participate in the annihilation process at freeze-out as, for example, flavor-changing neutral interactions that we also take into account (where the interactions were obtained from Ref. [27]). Then, essentially, we implement

[1]We are assuming normal hierarchy among the heavy neutral fermions N_1, N_2, and N_3 in such a way that N_1 is the lightest of them.

[2]From now on, we employ the notation of Ref. [8] for all the fields.

[3]However, even considering degenerate case (as done in Ref. [8]) the coannihilation channels are irrelevant.

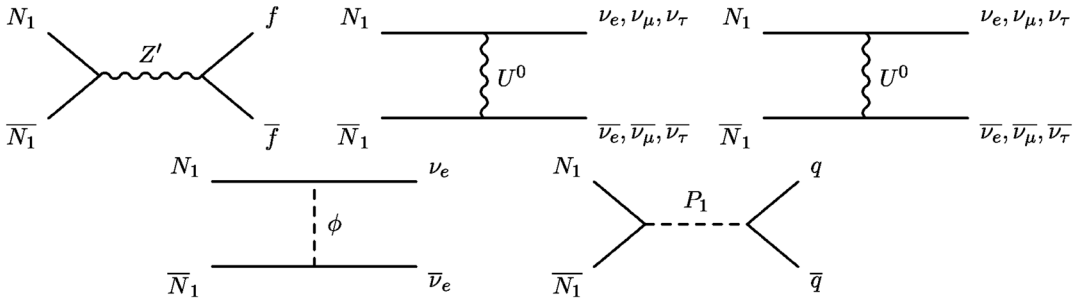

FIG. 1. The relevant processes that contribute to the abundance of N_1 with f representing the standard fermions.

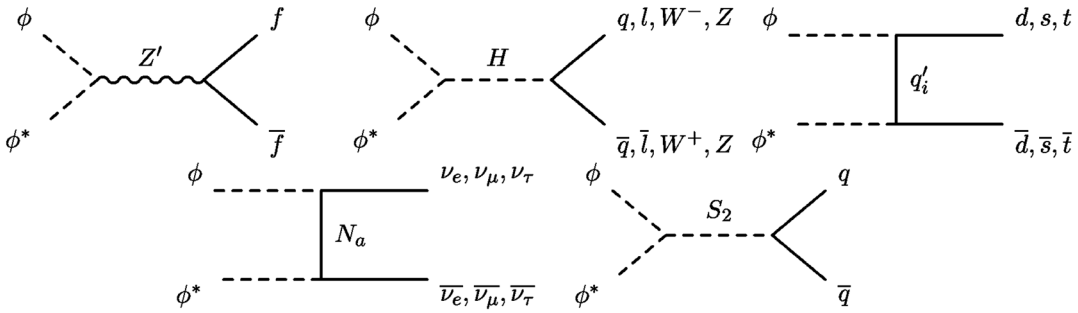

FIG. 2. The relevant processes that contribute to the abundance of ϕ with f, q, and l representing the standard quarks and charged leptons, respectively.

those interactions in the package CalcHEP [28] that furnishes the model files to be used in micrOMEGAs.

Firstly, we will handle the case where N_1 is the DM candidate. In the left panel of Fig. 3, we show its relic abundance for $M_{Z'} = 4$ TeV (blue curve), 5 TeV (green curve), and 6 TeV (cyan curve). We reinforce that in our calculation we took $M_{R-\text{oddparticles}} \gg M_{N_1}$, where $M_{R-\text{oddparticles}}$ represents the masses of all other R-odd particles. In that figure, the region in accordance with the Planck satellite [25], $\Omega h^2 = 0.11$, is shown by the red horizontal line. We can observe that the abundance of N_1 is suppressed when $M_{N_1} = M_{Z'}/2$, which means the resonance of Z'. This fact tells us that the processes mediated by the Z' boson are the most relevant ones. As the reader can see below, direct detection requires $M_{N_1} > 1900$ GeV. In summary, for this particular case, N_1 fulfills all the

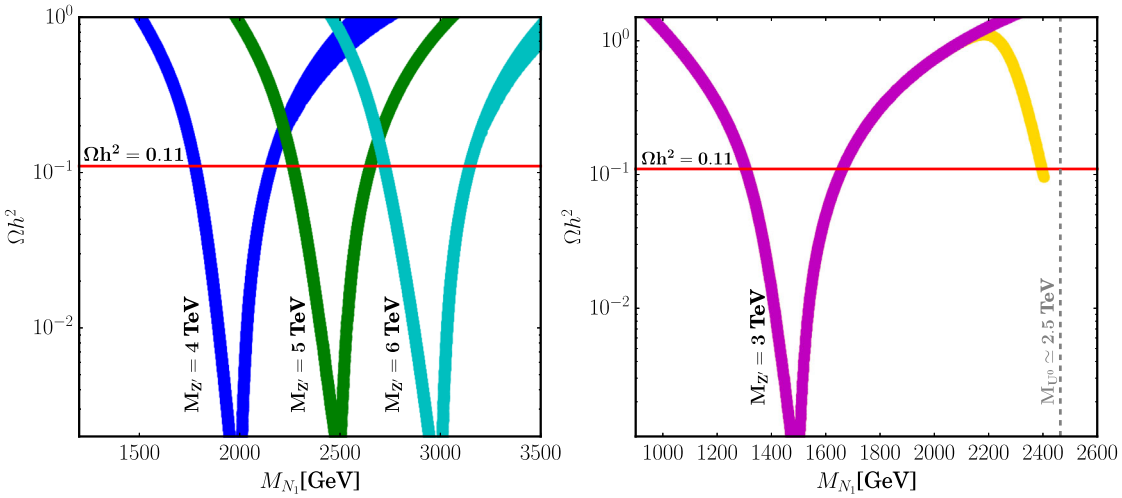

FIG. 3. Left panel: relic abundance for the heavy neutrino N_1 for $M_{Z'} = 4$ TeV (blue curve), 5 TeV (green curve), and 6 TeV (cyan curve). Right panel: relic abundance for the heavy neutrino N_1 for 3 TeV for $\Gamma_{P_1} = \mathcal{O}(1)$ GeV (pink curve) and $\Gamma_{P_1} = \mathcal{O}(10^{-3})$ GeV (yellow curve), showing the P_1 resonance. We vary the parameters λ_2, λ_3, and λ_6 given by Eq. (4) of the paper [8] always respecting the fact that $M_H = 125$ GeV (The expression for the Higgs mass involves λ_2, λ_3, and λ_6 as is shown in Eq. (12) of Ref. [8].).

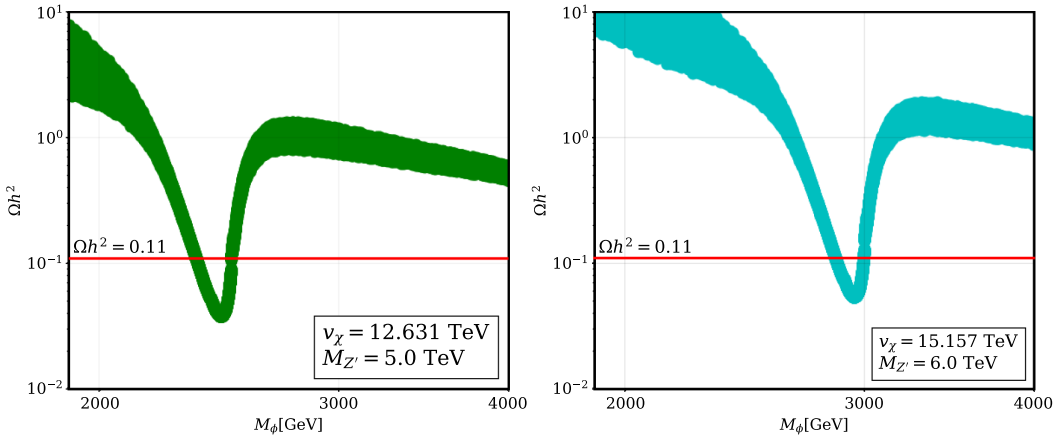

FIG. 4. The abundance of the scalar ϕ for two distinct values of $M_{Z'}$ (ν_χ). The left panel accounts for $M_{Z'} = 5.0$ TeV ($\nu_\chi = 12.631$ TeV), and the right panel accounts for $M_{Z'} = 6.0$ TeV ($\nu_\chi = 15.157$ TeV). The variation of M_ϕ (given by Eq. (14) of Ref. [8]) is achieved by varying λ_7. We also vary the parameters λ_2, λ_3, and λ_6 given by Eq. (4) of Ref. [8] always respecting the bound imposed by to $M_H = 125$ GeV.

conditions to be a dark matter candidate since it is stable and provides the correct abundance of dark matter in the Universe.

The interaction $\bar{\nu}_e N_1 U^0$ requires $M_{N_1} < M_{U^0}$ to guarantee the N_1 stability. This implies that always $M_{N_1} < M_{P_1}$. However, for some range of values of ν_χ, we can have $M_{U^0} \simeq M_{P_1}$, which implies that we can observe the appearance of P_1 resonance when $M_{N_1} \simeq M_{P_1}/2$, as is shown in the right panel of Fig. 3. The resonance only appears when $\Gamma_{P_1} \sim \mathcal{O}(10^{-3})$ GeV, which is represented by the yellow curve in the right panel of Fig. 3. However, our case gives $\Gamma_{P_1} \sim \mathcal{O}(1)$ GeV. Consequently, no one resonance can be observed, which is represented by the pink curve of the right panel in Fig. 3.

Let us now consider the case in which ϕ is the lightest R-odd particle. In Fig. 4, we show its relic abundance for the cases $M_{Z'} = 5$ TeV (green curve in left panel) and 6 TeV (cyan curve in right panel). The region in accordance with the Planck satellite [25], $\Omega h^2 = 0.11$, is shown by the red horizontal line. Observe that the abundance of ϕ is suppressed when $M_\phi = M_{Z'}/2$, which represents the resonance of Z'. This reveals to us that the processes mediated by Z' are the most relevant in this scenario. The reasons for which we display M_ϕ in Fig. 4 within the range 1.9 TeV $\leq M_\phi \leq 4$ TeV are twofold: direct detection excludes light ϕ, while the trilinear interaction $\phi H U^0$ imposes that $M_\phi <$ 4 TeV (in the left panel) and $M_\phi < 5$ TeV (in the right panel) in order to guarantee the stability of ϕ. In summary, ϕ fulfill all the requisites to constitute the dark matter of the Universe. It is important to note that the coupling of N_1 with Z' is approximately twice as large as the coupling of ϕ with Z'. Because of this, the suppression of the abundance of N_1 due to Z' resonance tends to be greater than ϕ.

Thus, we conclude that the model has two viable dark matter candidates that are exclusive unless degenerate in masses. We remark here that the model poses interactions among standard quarks (q) and Z' that change flavor [27,29–35]. We considered such contributions in the calculation of the abundance. As they are suppressed by the quark mixing matrix elements, then their contributions are irrelevant for the abundance in both cases of N_1 or ϕ as dark matter.[4]

B. Direct detection

The holy grail of direct dark matter detection is the assumption that the halo of Milk Way is composed by WIMPs and then an infinity of them passes through the Earth's surface each second. WIMPs have cross section of approximately weak strength, so it is to be expected that they interact weakly with the Standard Model particles; therefore, as the WIMPs are supposed to pass through the Earth, they can be directly detected by their interactions with the material (the nucleons, more precisely, the quarks) that compose the detector. The rate of interactions per unit of time per unit of mass of detector material, which can be simply expressed as [22]

$$R \simeq \frac{n\langle v\rangle\sigma}{m_N}, \tag{5}$$

where $\langle v\rangle$ is the average velocity of the incident WIMPs relative to the Earth frame, σ is the WIMP-nucleus cross section and m_N is the mass of target nucleus.

The WIMP interacts with the nucleus of the material that composes the detector and deposits an energy Q that is measured [1,36–42]. The WIMPs move in the halo with

[4]In regard to lepton flavor violation processes like $\mu \to e\gamma$, once we are considering $N_{1,2,3}$ in a diagonal basis, neither N_i nor W' contributes to such processes. Then, we do not need to worry about this here.

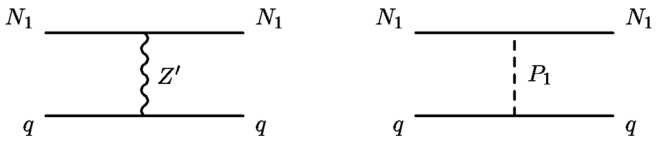

FIG. 5. Processes which contribute to the WIMP-nucleon cross section of N_1.

velocities determined by their velocity distribution function $f(v)$; then, the differential scattering event rate can be written

$$dR = \left(\frac{\rho_0 \sigma_0}{2 m_{\rm DM} \mu_N^2}\right) F^2(Q) \int \frac{f(v)}{v} dv dQ, \tag{6}$$

where ρ_0 is the WIMP density near the Earth, $m_{\rm DM}$ is the DM mass, σ_0 is the WIMP-nucleus cross section ignoring the form factor suppression $F(Q)$, and $\mu_N = m_{\rm DM} m_N/(m_N + m_{\rm DM})$ is the reduced WIMP-nucleus mass.

As discussed above, the interactions among dark matter and Z' are the most relevant ones. Because of the features of these interactions, we will have two types of WIMP-nucleus interactions: spin independent (SI) and spin dependent. It is very well known that the SI ones are the ones we must take into account. Then, we will probe here the limits on the SI cross section of N_1 and ϕ.

The spin independent WIMP-nucleus cross section at zero momentum transfer can be expressed as [1,22,26]

$$\sigma_0 = \frac{4\mu_N^2}{\pi} (Z f_p + (A - Z) f_n)^2, \tag{7}$$

where Z is the atomic number, A is the atomic mass, and f_p and f_n are effective couplings with protons and neutrons, respectively, and depend of the particle physics input of a given model. In most cases, the couplings to protons and neutrons are approximately equal, $f_p \cong f_n$; then,

$$\sigma_0 = \sigma^{\rm SI} \frac{\mu_N^2}{\mu_n^2} A^2, \tag{8}$$

where μ_n is the WIMP-nucleon reduced mass and

$$\sigma^{\rm SI} = \frac{4\mu_n^2}{\pi} (f^n)^2, \tag{9}$$

with $f^n = f_{n,p}$, which is also called WIMP-nucleon amplitude. Experiments tend to constraint the $\sigma^{\rm SI}$, which is nucleus independent.

The processes which contribute to the spin-independent cross section of N_1 are shown in Fig. 5. In our calculation, we took into account both contributions; however, we remark that the process mediated by the pseudoscalar P_1 is completely negligible in comparison to the one mediated by Z'. This is so because its coupling involves a γ_5 and is suppressed by a tiny Yukawa coupling; see Ref. [8]. Additionally, in Fig. 6, we have the processes which contribute to spin-independent cross section of ϕ. Our results were obtained by implementing all these interactions in CalcHEP. We made use of micrOMEGAs to compute $\sigma^{\rm SI}$ through Eq. (9).

After discussing a little bit about the direct detection method and showing the processes which contribute to the WIMP-nucleus cross section, we are able to show and analyze the results for each candidate.

The main results of this work are shown in Fig. 7, which consider the recent PandaX-4T result [4] (in agreement with Fig. 4 of Ref. [4]). In the left panel of Fig. 7, we present our numerical results for N_1-nucleon cross section as a function of M_{N_1} for $M_{Z'} = 4$ TeV (blue curve), 5 TeV (green curve), and 6 TeV (cyan curve). To guarantee the stability of N_1, due to the trilinear interaction $\nu_e N_1 U^0$, we needed to assume $M_{N_1} < M_{U^0}$. This is the reason why the blue line in the left panel of Fig. 7 goes up to $M_{N_1} = 3200$ GeV. The black dashed line represents the upper limit imposed by the recent direct detection PandaX-4T experimental result. The region above the dashed line is excluded by the PandaX-4T bound. The red triangles represent the right amount of relic abundance. Then, as the red triangles that overlap the blue line lie above the black dashed line, we conclude that the correct abundance and PandaX-4T bound exclude Z' with mass of 4 TeV.

In the right panel of Fig. 7, we present our numerical results for ϕ-nucleon cross section as a function of M_ϕ for

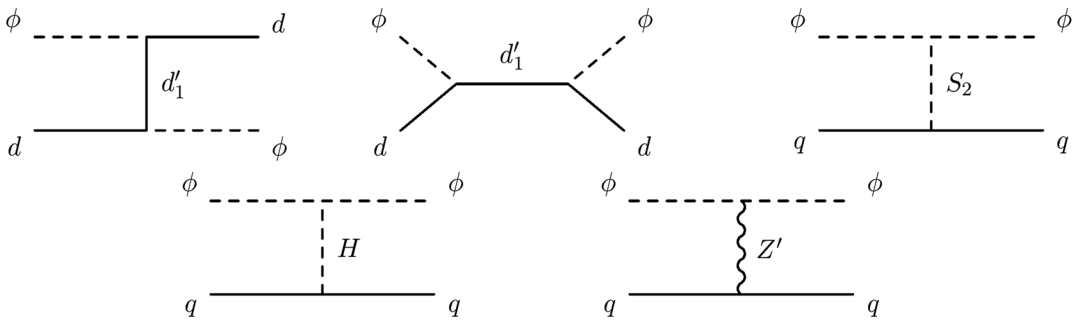

FIG. 6. Processes which contribute to the WIMP-nucleon cross section of ϕ.

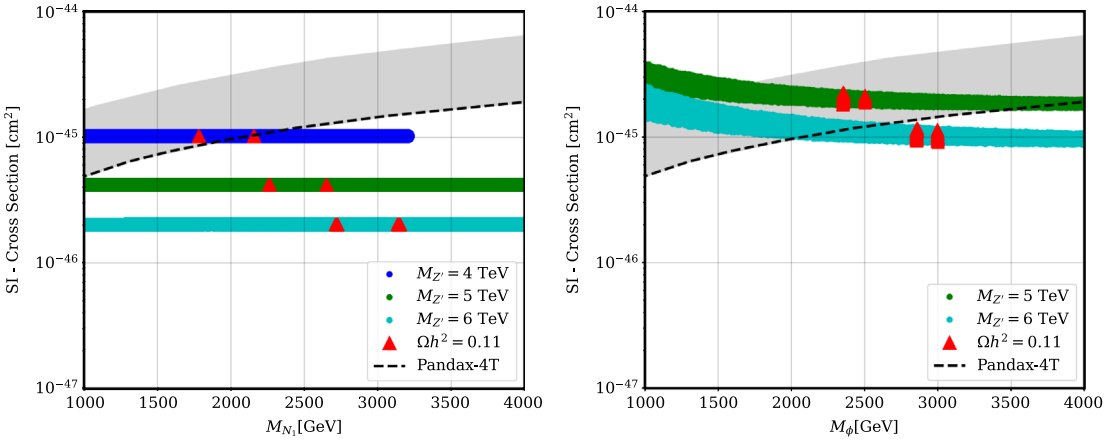

FIG. 7. The WIMP-nucleon cross section for N_1 (left panel) and ϕ (right panel). The red triangles represents the right DM abundance, for both cases. The black dashed line represents the upper limit imposed by the direct detection experiment PandaX-4T [4]. The light gray band represents the $\pm 1\sigma$ sensitivity band, which is in agreement with Fig. 4 of Ref. [4].

two values of $M_{Z'}$. As we can see in this figure, the correct abundance and PandaX-4T bound exclude Z' with mass of 5 TeV for any value of M_ϕ.

As noted in both panels of Fig. 7, the allowed value of the mass of Z' is related to the mass of the dark matter candidate. Then, in Fig. 8, we present the region of parameter space $(M_{Z'}, M_{(N_1,\phi)})$, which is allowed by the recent PandaX-4T. In both figures, we can see, represented by the blue region, all the values of the parameter space $(M_{Z'}, M_{(N_1,\phi)})$ that respect PandaX-4T and have the correct abundance. Thus, we have a lower bound on the mass of Z' depending on the mass of the dark matter candidate. For the case in which N_1 is the dark matter candidate, we have that the lower bound on the mass of Z' is $M_{Z'} = 4.1$ TeV for $M_{N_1} = 2.2$ GeV. It is represented by the dashed black line in the left panel of Fig. 8. For the case where ϕ is the dark matter candidate, we have that the lower bound on the mass of Z' is $M_{Z'} = 5.7$ TeV for $M_\phi = 2.9$ TeV.

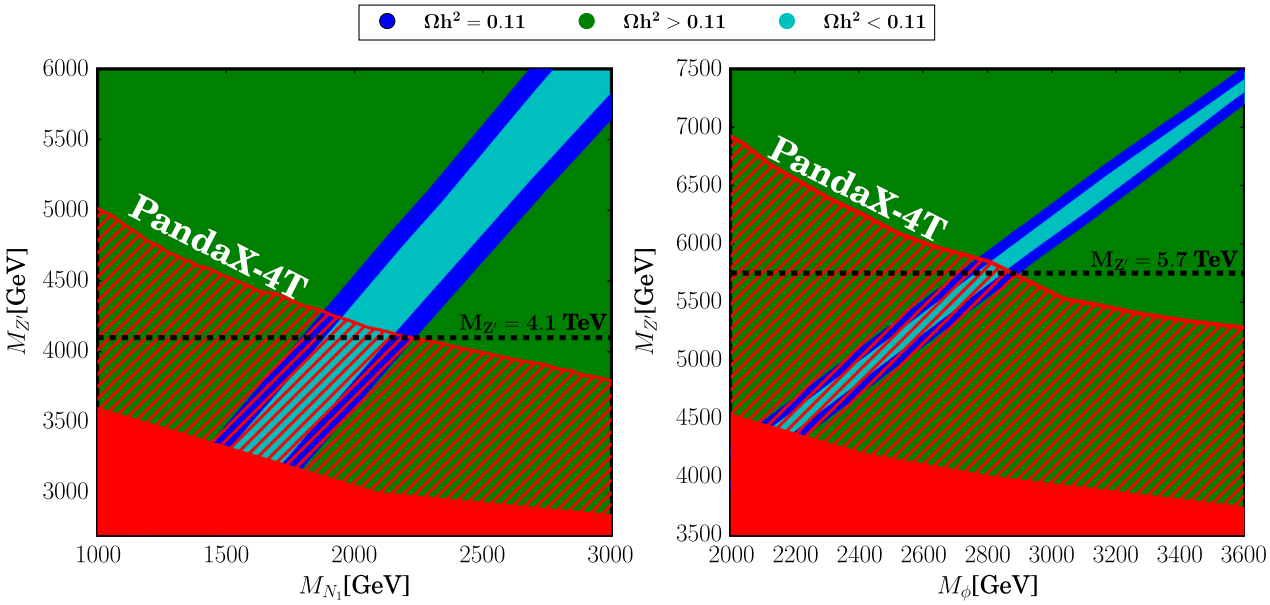

FIG. 8. Viable parameter space for the DM candidates N_1 (left panel) and ϕ (right panel) in the plane $(M_{Z'}, M_{N_1})$ and $(M_{Z'}, M_\phi)$, respectively. In both panels, the correct dark matter relic density ($\Omega h^2 = 0.11$) is represented by blue region, the cyan region represents the underabundance ($\Omega h^2 < 0.11$) parameter space, and the green region represents the overabundance ($\Omega h^2 > 0.11$) parameter space. The red line represents the PandaX-4T direct detection experiment with its $\pm 1\sigma$ sensitivity band represented by the hatched red area. The red region is excluded by the PandaX-4T direct detection experiment.

IV. CONCLUSIONS

In this work, we investigated the implications of PandaX-4T bound on the parameters of the dark matter candidates of the 3-3-1LHN model. First of all, the PandaX-4T bound is not compatible with light dark matter. In our model, when we assume that N_1 is the dark matter candidate, the PandaX-4T bound requires $M_{N_1} \geq 1.9$ TeV. For the other case where ϕ is the dark matter candidate, we get $M_\phi \geq 2.8$ TeV.

Another interesting result is that, due to the fact that all relevant processes are mediated by Z', the PandaX-4T bound may be translated into a lower bound on Z' mass but now related to the mass of the dark matter candidate. As shown in the left panel of Fig. 8, the lower bound on the mass of Z' is $M_{Z'} \geq 4.1$ TeV ($v_\chi \geq 10357$ GeV), but this requires $M_{N_1} = 2200$ GeV. In the case where ϕ is the dark matter candidate, this lower bound is yet even more restrictive, rendering $M_{Z'} \geq 5.7$ TeV ($v_\chi \geq 14400$ GeV) for $M_\phi = 2.9$ TeV. Observe that the bound on $M_{Z'}$ is more severe for the ϕ scenario. We highlight that the lower bound on $M_{Z'}$ obtained here turns out to be more restrictive than previous works existing in the literature [8], including that imposed by the LHC [43–46].[5] Of course, we are aware that such a bound on $M_{Z'}$ is an implication of the assumption that N_1 or ϕ is the candidate for the dark matter of the Universe. A recent work on the subject, see Ref. [48], found that future hadron colliders may severely restrict $M_{Z'}$. If this is realized, then, according to Fig. 8, N_1 and ϕ must be heavier in order to give the correct abundance.[6] We finalize saying that the PandaX-4T bound put the dark matter candidates of the 3-3-1LHN model in a scale of energy that cannot be probed by the LHC in the present running and pushed the lower bound on the mass of Z' for a scale that surpasses the existing bound.

ACKNOWLEDGMENTS

C. A. S. P. was supported by the CNPq research Grant No. 304423/2017-3, and V. O. was supported by CAPES.

[5]For other source of constraint on the mass of Z', see Ref. [47].

[6]We recall that there is an upper limit for the WIMP mass that arises from the question of unitarity; see Ref. [49].

[1] R. W. Schnee, in *Theoretical Advanced Study Institute in Elementary Particle Physics: Physics of the Large and the Small* (World Scientific, Singapore, 2011), pp. 775–829.
[2] M. Battaglia, I. Hinchliffe, and D. Tovey, J. Phys. G **30**, R217 (2004).
[3] G. Bélanger, E. Nezri, and A. Pukhov, Phys. Rev. D **79**, 015008 (2009).
[4] Y. Meng *et al.* (PandaX-4T Collaboration), Phys. Rev. Lett. **127**, 261802 (2021).
[5] M. Dutra, V. Oliveira, C. A. de S. Pires, and F. S. Queiroz, J. High Energy Phys. 10 (2021) 005.
[6] H. N. Long, D. V. Soa, V. H. Binh, and A. E. Cárcamo Hernández, arXiv:2007.05004.
[7] J. K. Mizukoshi, C. A. de S. Pires, F. S. Queiroz, and P. S. Rodrigues da Silva, Phys. Rev. D **83**, 065024 (2011).
[8] S. Profumo and F. S. Queiroz, Eur. Phys. J. C **74**, 2960 (2014).
[9] D. Cogollo, A. X. Gonzalez-Morales, F. S. Queiroz, and P. R. Teles, J. Cosmol. Astropart. Phys. 11 (2014) 002.
[10] P. V. Dong, C. S. Kim, D. V. Soa, and N. T. Thuy, Phys. Rev. D **91**, 115019 (2015).
[11] G. Arcadi, C. P. Ferreira, F. Goertz, M. M. Guzzo, F. S. Queiroz, and A. C. O. Santos, Phys. Rev. D **97**, 075022 (2018).
[12] P. V. Dong, H. T. Hung, and T. D. Tham, Phys. Rev. D **87**, 115003 (2013).
[13] D. T. Huong, C. S. Kim, H. N. Long, and N. T. Thuy, arXiv:1110.1482.
[14] A. E. Cárcamo Hernández, D. T. Huong, and H. N. Long, Phys. Rev. D **102**, 055002 (2020).
[15] C. E. Alvarez-Salazar, O. L. G. Peres, and B. L. Sánchez-Vega, Astron. Nachr. **340**, 135 (2019).
[16] J. C. Montero, A. Romero, and B. L. Sánchez-Vega, Phys. Rev. D **97**, 063015 (2018).
[17] J. G. Ferreira, C. A. de S. Pires, J. G. Rodrigues, and P. S. Rodrigues da Silva, Phys. Lett. B **771**, 199 (2017).
[18] F. Queiroz, C. A. de S. Pires, and P. S. R. da Silva, Phys. Rev. D **82**, 065018 (2010).
[19] F. Pisano and V. Pleitez, Phys. Rev. D **46**, 410 (1992).
[20] H. N. Long, Phys. Rev. D **53**, 437 (1996).
[21] C. A. de S. Pires and P. S. Rodrigues da Silva, J. Cosmol. Astropart. Phys. 12 (2007) 012.
[22] G. Jungman, M. Kamionkowski, and K. Griest, Phys. Rep. **267**, 195 (1996).
[23] J. Cooley, SciPost. Lect. Notes 55 (2022).
[24] K. Griest and D. Seckel, Phys. Rev. D **43**, 3191 (1991).
[25] N. Aghanim *et al.* (Planck Collaboration), Astron. Astrophys. **641**, A6 (2020).
[26] G. Bélanger, F. Boudjema, A. Goudelis, A. Pukhov, and B. Zaldivar, Comput. Phys. Commun. **231**, 173 (2018).
[27] H. N. Long and V. T. Van, J. Phys. G **25**, 2319 (1999).
[28] A. Belyaev, N. D. Christensen, and A. Pukhov, Comput. Phys. Commun. **184**, 1729 (2013).
[29] J. T. Liu, Phys. Rev. D **50**, 542 (1994).
[30] J. A. Rodriguez and M. Sher, Phys. Rev. D **70**, 117702 (2004).
[31] R. H. Benavides, Y. Giraldo, and W. A. Ponce, Phys. Rev. D **80**, 113009 (2009).

[32] J. M. Cabarcas, D. Gomez Dumm, and R. Martinez, J. Phys. G **37**, 045001 (2010).
[33] J. M. Cabarcas, J. Duarte, and J.-A. Rodriguez, Adv. High Energy Phys. **2012**, 657582 (2012).
[34] D. Cogollo, A. V. de Andrade, F. S. Queiroz, and P. Rebello Teles, Eur. Phys. J. C **72**, 2029 (2012).
[35] A. C. B. Machado, J. C. Montero, and V. Pleitez, Phys. Rev. D **88**, 113002 (2013).
[36] M. Taoso, G. Bertone, and A. Masiero, J. Cosmol. Astropart. Phys. 03 (2008) 022.
[37] D. Hooper, in *Theoretical Advanced Study Institute in Elementary Particle Physics: The Dawn of the LHC Era* (World Scientific, Singapore, 2010), pp. 709–764.
[38] C. Munoz, Int. J. Mod. Phys. A **19**, 3093 (2004).
[39] G. Bertone, D. Hooper, and J. Silk, Phys. Rep. **405**, 279 (2005).
[40] J. Gascon, Nucl. Instrum. Methods Phys. Res., Sect. A **520**, 96 (2004).
[41] Y. Ramachers, Nucl. Phys. B, Proc. Suppl. **118**, 341 (2003).
[42] C.-L. Shan, Theoretical Interpretation of Experimental Data from Direct Dark Matter Detection, Other thesis, 2007, arXiv:0707.0488.
[43] E. Ramirez Barreto, Y. A. Coutinho, and J. Sa Borges, Phys. Lett. B **689**, 36 (2010).
[44] E. Ramirez Barreto, Y. do Amaral Coutinho, and J. Sa Borges, Eur. Phys. J. C **50**, 909 (2007).
[45] E. Ramirez Barreto, Y. do Amaral Coutinho, and J. Sa Borges, arXiv:hep-ph/0605098.
[46] Y. A. Coutinho, V. Salustino Guimarães, and A. A. Nepomuceno, Phys. Rev. D **87**, 115014 (2013).
[47] H. N. Long and T. Inami, Phys. Rev. D **61**, 075002 (2000).
[48] A. Alves, L. Duarte, S. Kovalenko, Y. M. Oviedo-Torres, F. S. Queiroz, and Y. S. Villamizar, arXiv:2203.02520.
[49] K. Griest and M. Kamionkowski, Phys. Rev. Lett. **64**, 615 (1990).